Microelectromechanical devices driven by thermosalient effects

Jad Mahmoud Halabi, Isabelle Séguy, Ludovic Salvagnac, Panče Naumov, Thierry Leichle, Fabrice Mathieu, Benjamin Duployer, Durga Prasad Karothu, Liviu Nicu

Cell Reports
Physical Science

CellPress
OPEN ACCESS

Article

Microelectromechanical devices driven by thermosalient effects

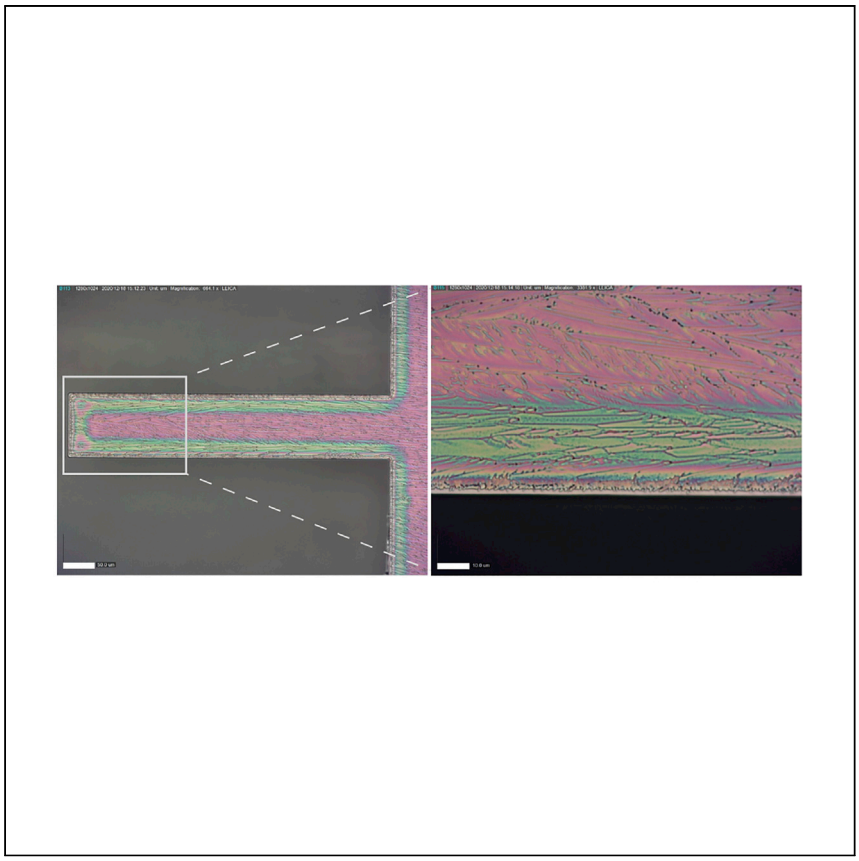

In this work, Mahmoud Halabi et al. integrate soft organic crystalline thin films with rapid responsiveness to thermal conditions as active elements in hybrid devices, thereby combining thermomechanical and piezoelectric properties to enhance actuating and sensing capacities of microdevices.

Jad Mahmoud Halabi, Isabelle Séguy, Ludovic Salvagnac, ..., Durga Prasad Karothu, Liviu Nicu, Panče Naumov

nicu@laas.fr (L.N.)
pance.naumov@nyu.edu (P.N.)

Highlights

New organic actuating materials in hybrid MEMS devices

Controllable and scalable thin-film fabrication of dynamic molecular crystals

Preservation of thermosalient phase transitions in thin films of molecular crystals

Rapid mechanical response driven by thermal changes for actuation/sensing

Mahmoud Halabi et al., Cell Reports Physical Science *3*, 101133
November 16, 2022
https://doi.org/10.1016/j.xcrp.2022.101133

Please cite this article in press as: Mahmoud Halabi et al., Microelectromechanical devices driven by thermosalient effects, Cell Reports Physical Science (2022), https://doi.org/10.1016/j.xcrp.2022.101133

Cell Reports
Physical Science

Article

Microelectromechanical devices driven by thermosalient effects

Jad Mahmoud Halabi,[1] Isabelle Séguy,[2] Ludovic Salvagnac,[2] Thierry Leïchlé,[2,3] Daisuke Saya,[2] Fabrice Mathieu,[2] Benjamin Duployer,[4] Durga Prasad Karothu,[1] Liviu Nicu,[2,*] and Panče Naumov[1,5,6,7,*]

SUMMARY

The state-of-the-art microelectromechanical systems (MEMSs) technology faces challenges in meeting the requirements of the next decade regarding improved performance, functionality, and power consumption, which can be addressed by resorting to new actuating materials. Dynamic molecular single crystals have been explored as actuating elements; however, difficulties with control over the geometry and fabrication of these materials has limited their scalability and application. Here, we present dynamic molecular crystals driven by thermosalient phase transitions as alternative materials in MEMSs technology with swift and amplified mechanical response. This work employs a thermally deposited stable polycrystalline thin film of L-pyroglutamic acid to fabricate a prototypical thermosalient organic crystal-MEMS (TS-OC-MEMS). The organic thin film undergoes a reversible and cyclable martensitic phase transition that drives the deformation. The TS-OC-MEMSs provide a reliable and scalable solution to utilize dynamic molecular crystals in robust applications and circumvent the challenges that have long stifled their application as actuating materials.

INTRODUCTION

Molecular crystals, composed of covalently bonded light atoms that form discrete and highly ordered molecules bound through intermolecular forces, exhibit mechanically responsive properties that have increasingly positioned them as moderately soft smart materials with a promising actuating potential. The utility of the unique properties of dynamic molecular crystals in practical applications has been recently demonstrated in dynamic cantilevers,[1,2] ratchets,[3] optical waveguides,[4–11] and shape-shifting and gear-like elements.[12] However, most of these applications remain on a small scale, are built *ad hoc*, and usually serve as a proof of concept that underpins the ability of dynamic molecular crystals to convert energy into work. Organic crystals have also been explored for their electrical and fast switching properties in cross-wire circuits and nanowires,[13] electrical photo- or thermo-switching circuitry,[14] organic transistors, and diodes.[15–17] Additionally, the responsive and flexible structures of molecular crystals have also been studied as gas and vapor sensors,[18] ionizing radiation and X-ray detectors,[19] and organic photosynaptic and optical sensing devices.[20] Organic crystals have been studied for their unique electromechanical properties and considered as alternative materials in flexible, wearable, and disposable electronics and semiconductor applications.[21,22] Despite the plethora of attempts to utilize the combination of unique optical, thermal, electrical, and mechanical properties of molecular single crystals,

[1]Smart Materials Lab, New York University Abu Dhabi, PO Box 129188, Abu Dhabi, United Arab Emirates

[2]LAAS-CNRS, Toulouse, France

[3]IRL2958 Georgia-Tech CNRS, Atlanta, GA, USA

[4]CIRIMAT, Université de Toulouse, Toulouse, France

[5]Center for Smart Engineering Materials, New York University Abu Dhabi, PO Box 129188, Abu Dhabi, United Arab Emirates

[6]Molecular Design Institute, Department of Chemistry, New York University, 100 Washington Square East, New York, NY 10003, USA

[7]Lead contact

*Correspondence: nicu@laas.fr (L.N.), pance.naumov@nyu.edu (P.N.)

https://doi.org/10.1016/j.xcrp.2022.101133

regrettably, most of these applications have not yet materialized into robust and functional devices.

Aside from the lack of proper performance characterization, some of the main pitfalls in introducing molecular crystals into applications lie in the repeated over-focusing on these structures as stand-alone elements in the related reports. Difficulties with establishing reproducible crystallization procedures with predictable and standardized crystal habits (characteristic external shape of a crystal) and sizes, lack of compatibility in mechanical properties when coupled with other more rigid components, and significant proneness to fatigue and wear over multiple cycles and prolonged usage all stand in the way of implementing molecular single crystals as reliable actuating elements in devices. The so-called salient effects that can be induced by heat, light, or pressure are a collection of mechanical effects exhibited by some molecular crystals that are usually observed as rapid self-propulsion, splintering, or even explosion that leads to complete disintegration. These effects, now documented in over 30 molecular crystals,[23–31] are considered the fastest mechanical response and the most robust exhibition of actuation of ordered organic solids.[32] The transformations are sufficiently fast to generate acoustic signals as shock waves through the crystal that can be detected and analyzed.[33] The capacity of the salient solids for rapid locomotion or blasting is due to fast martensitic transitions in their structures,[34] which are preceded by lattice softening.[35] These transitions nucleate at high thermally induced stress sites and propagate through the crystal structure in a diffusionless manner. The progression of the phase front occurs on a scale of a millisecond or faster.[36] Given the speed of transformation, the resultant elastic energy induced by the accumulated molecular strain at a certain threshold can no longer be effectively dissipated throughout the crystal structure while allowing the rearrangement of molecules into a coherent crystal packing. In cases where the reconfigured molecules fail to re-establish a strong network of intermolecular interactions, the integrity of the crystal is usually compromised, causing its shattering or disintegration. This effect is particularly common with crystals that have comparable dimensions along different crystal axes. Such crystals have lower surface area per unit volume relative to their rod-shaped counterparts, further contributing to the rigidity and hindrance of free molecular reconfiguration.

Electromechanical devices fabricated using advanced microscale and nanoscale technologies were initially used as platforms for micromechanical characterization of materials. Since then, they have been dedicated to analyzing, sensing, and identifying specific biological entities[37] or detecting small chemical species.[38,39] Although industrial success stories are well established in the field of physical sensors, the interest in scientific inquiry related to the conventional microelectromechanical system (MEMS) realm appears to have decreased. Today, the main outlet for MEMS devices is their use as actuation/sensing devices, a state that indirectly limits the room for innovation beyond the quest for new functional materials with enhanced responsive capacities and unique properties. Organic small molecules offer the advantageous opportunity to use thermal evaporation techniques from effusion cells for deposition. Usually, a high vacuum is used (about 10^{-6} mbar or lower) to obtain highly reproducible and pure organic thin films while attaining an accurate deposition rate and control over the film thickness. These vacuum processes are widely used in organic electronics device fabrication, for example, the production of organic light-emitting diodes.

In this paper, and for the first time, we explore the application of thermosalient molecular crystals in the form of thin films in MEMS devices. We investigate the ability of

Please cite this article in press as: Mahmoud Halabi et al., Microelectromechanical devices driven by thermosalient effects, Cell Reports Physical Science (2022), https://doi.org/10.1016/j.xcrp.2022.101133

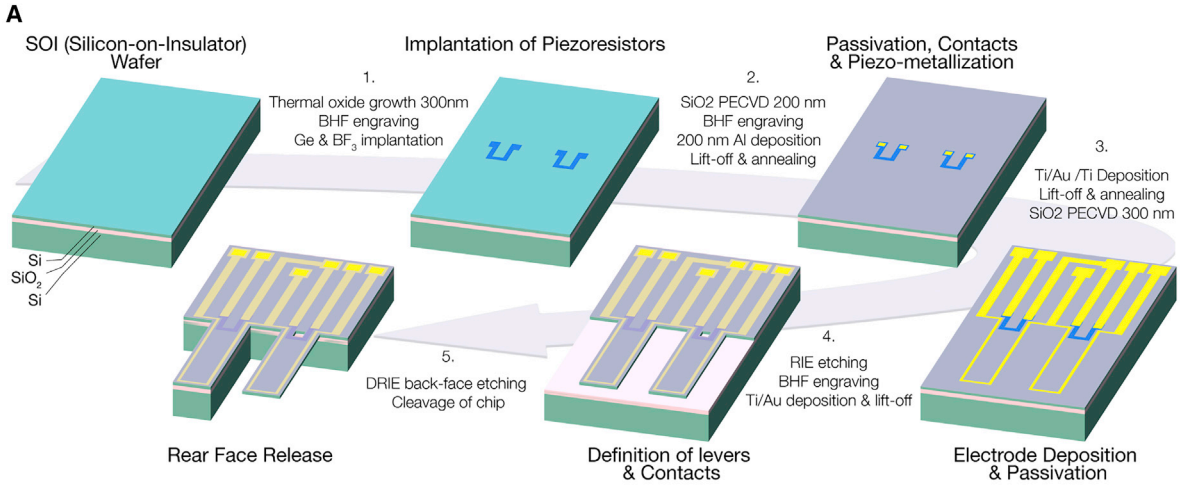

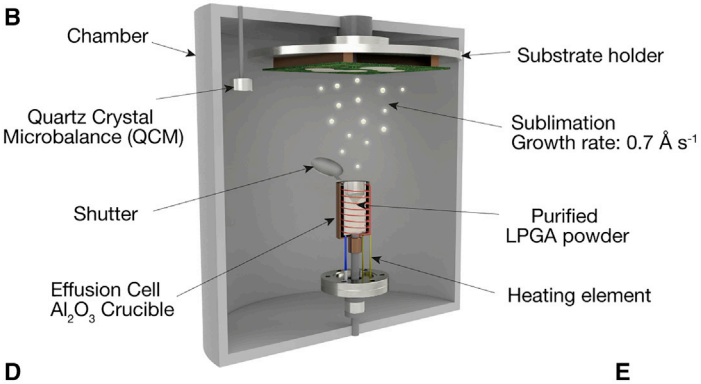

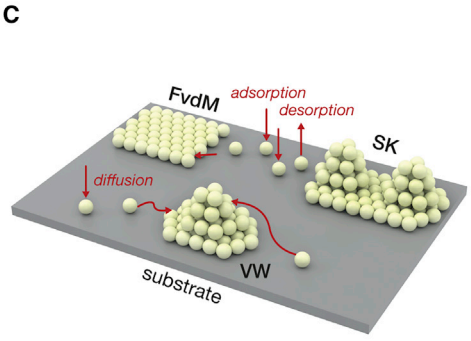

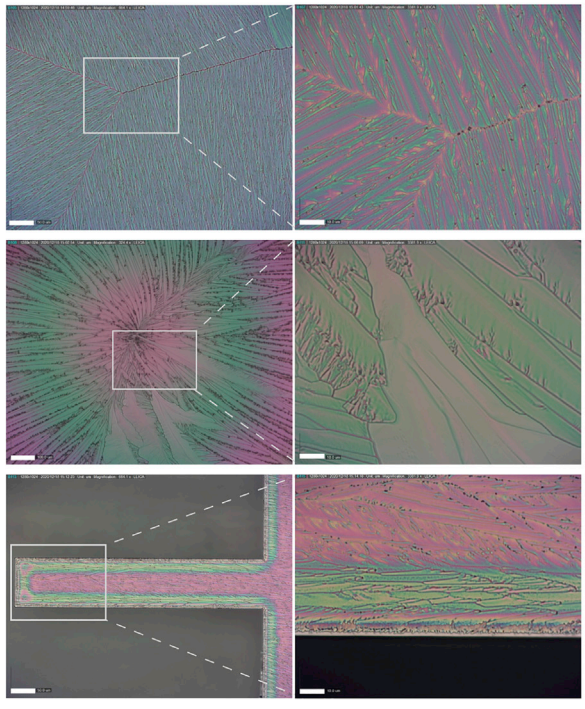

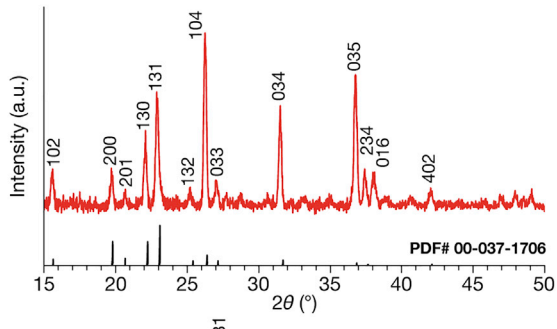

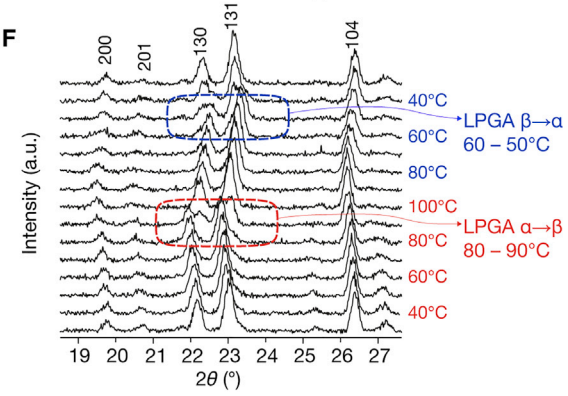

Figure 1. Fabrication of the MEMS device, LPGA thermal deposition, topology of the LPGA crystalline thin film, and X-ray diffraction analysis
(A) Schematic of the step-by-step fabrication process of microcantilevers with sensing and actuation capabilities.
(B) Thermal evaporation setup.
(C) FvdM (Frank van der Merwe layer-by-layer growth), VW (Volmer-Weber island growth), and SK (Stranski-Krastanov layer-by-layer followed by island growth) modes of nucleation and epitaxial growth of thin films deposited through thermal evaporation.
(D) Optical images of the continuous and polycrystalline LPGA thin film. The scale bars for each zoom-in represent 50 μm (top left and bottom left), 10 μm (top right, middle right, and bottom right), and 100 μm (middle left).
(E) Powder X-ray diffraction pattern of LPGA crystalline film.
(F) Peak shift due to the phase transition at heating and cooling of the LPGA thin film.

the high surface-area-to-volume ratios to enable a large deformation phase transition, lower the thermodynamic transformation free-energy barrier, and preserve the integrity of the material by mitigating excessive stresses that are absorbed by hydrogen bonding. The polycrystalline organic thin film integrated into the fabricated TS-OC-MEMS device drives a reversible and cyclable mechanical deformation than can be triggered by heat because of its thermosalient properties. Within a broader context, this work aims to introduce new materials into well-studied micromechanical systems and test new fabrication methods for molecular crystals as thin films that are considered better suited for applications relative to single crystals.

RESULTS AND DISCUSSION

Thin-film deposition and characterization

A hybrid thermosalient organic crystal-MEMS (TS-OC-MEMS) device composed of active microcantilevers (MC-As) with sensing and actuating capabilities was fabricated on which a thermosalient thin film of polycrystalline L-pyroglutamic acid (LPGA) was deposited through thermal evaporation (Figures 1A–1C; for additional details, see experimental procedures and Note S1). To optimize the conditions for thermal evaporation and to characterize the properties of the organic polycrystalline film, we used a thermal evaporation setup shown in Figure 1B to deposit LPGA on passive microcantilevers (MC-Ps) fabricated from bare silicon (see Figure S1A; supplemental information). Given that the silicon's surface free energy is lower than the sum of LPGA substrate free energy and the interfacial LPGA/Si free energy, a Volmer-Weber or island growth mode of the thin film was dominant at low film thickness, leading to discontinuous films. Increasing the thickness of deposited LPGA above a critical thickness of 100 nm contributed to a more homogeneous, layered growth of a continuous thin film that covered the entire surface. Under a polarizing microscope, the film showed large domains with clearly visible dividing boundaries, indicating that the otherwise macroscopically continuous thin film is polycrystalline. Figure 1D shows a focal point where the crystallization appears to have been initiated and radially progressed, as well as color gradients that reflect the varying thickness in the film. The thickness gradient is optically visible with varying thickness around the edges compared with the center of the cantilever; however, the film still appears to be continuous and covers the entire surface. The thin film was also scanned using atomic force microscopy (AFM) to determine the average thickness, which was found to be $t_{avg} \approx 600$ nm across the deposited layer (see Figure S2; supplemental information).

Figure 1E shows an X-ray diffractogram of a 600 nm LPGA film. The diffraction peaks shown correspond to those of LPGA powder and confirm the crystallinity of the sample.[40] The absence of other diffraction peaks also demonstrates the purity of the thin film; however, because of the prestressed state of the film and its texture, there is an angular offset and different intensity ratios from the reference. The LPGA film was analyzed by variable-temperature X-ray diffraction to determine whether it undergoes a phase transition because it has been previously reported on LPGA

Please cite this article in press as: Mahmoud Halabi et al., Microelectromechanical devices driven by thermosalient effects, Cell Reports Physical Science (2022), https://doi.org/10.1016/j.xcrp.2022.101133

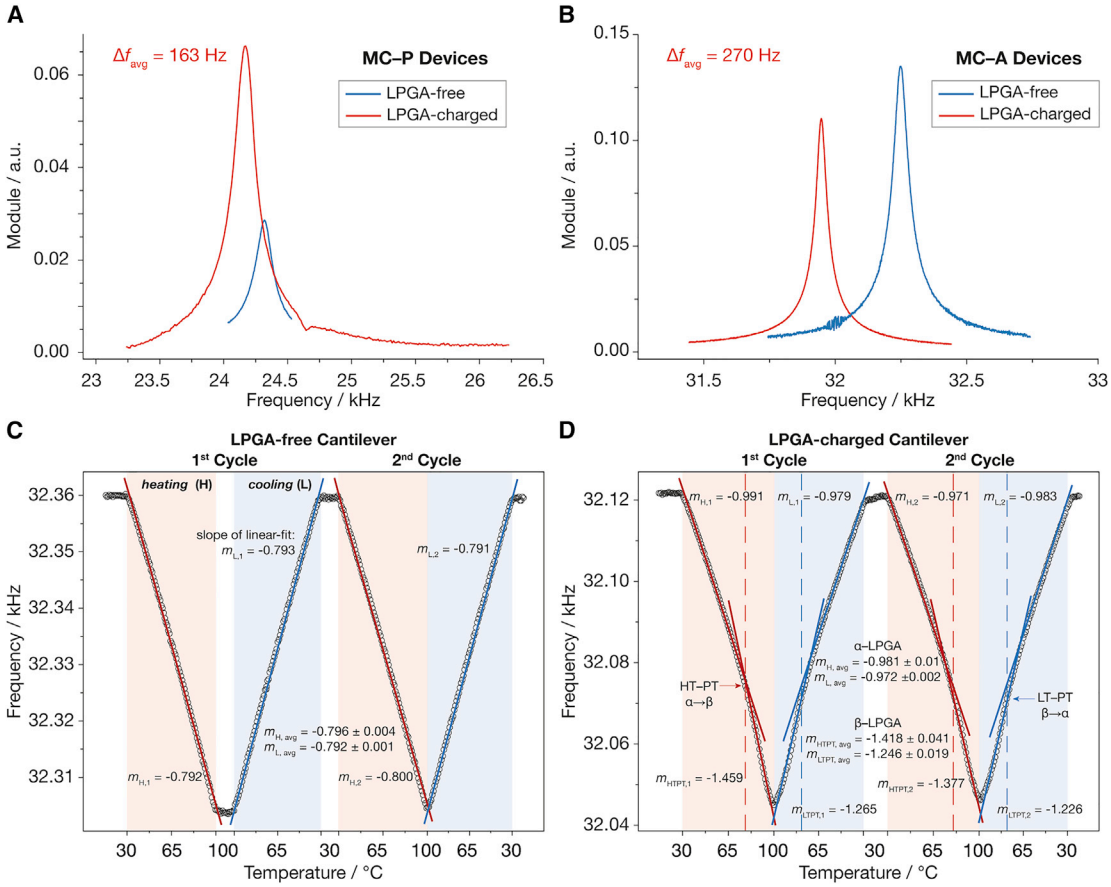

Figure 2. Resonant frequency shift and change with respect to temperature

(A and B) Dynamic frequency measurements on LPGA-free and LPGA-charged MC-P and MC-A devices, respectively.

(C and D) The change of resonance frequency of (C) LPGA-free cantilever and (D) LPGA-charged cantilever with respect to temperature during two cycles of consecutive heating and cooling. The high-temperature and low-temperature phase transitions in the LPGA-charged cantilever are apparent given the abrupt change in the slope of the linear regressions plotted.

powder.[41] Figure 1F shows the different diffractograms of the film as a function of temperature. From 30°C to 80°C, all the diffraction peaks shift toward lower 2θ values. This well-known phenomenon is due to the thermal expansion of the crystal lattice with increasing temperature. Between 80°C and 90°C, the (130) and (131) peaks undergo a sudden shift toward higher 2θ values, indicating the decrease in the *b* axis in the orthorhombic structure[41] of the LPGA film. This behavior is characteristic of the $\alpha \rightarrow \beta$ transition of LPGA. During cooling, the material exhibits another phase transition around 60°C, indicating the reverse transition $\beta \rightarrow \alpha$.

To characterize the mechanical properties of the LPGA thin film, we performed resonance frequency measurements before and after the deposition of 100 nm LPGA film on a series of six 5-μm-thick MC-P cantilevers (see experimental procedures and Figure S3; supplemental information). Figure 2A shows an average resonance frequency shift $\Delta f = 163 \pm 44$ Hz between the LPGA-free and LPGA-charged MC-P cantilevers. According to the conventional beam theory, the resonant frequency of a monolithic cantilever beam for the fundamental vibrational mode in bending can be expressed as[42]

$$f_i = \frac{1}{2\pi} \cdot \left(\frac{1.875}{L}\right)^2 \cdot \sqrt{\frac{EI}{\rho A}}, \qquad \text{(Equation 1)}$$

where E is the Young's modulus, I is the moment of inertia, ρ is the density, and A is the cross-sectional area. Considering that the LPGA-charged cantilever can be modeled as a simple long and slender bilayer beam, the Young's modulus of the LPGA thin film can be calculated as

$$\left(\frac{f_{bi}}{f_s}\right)^2 = \frac{(E_r t_r^3 + 1)(E_r t_r + 1) + 3E_r t_r (t_r + 1)^2}{(\rho_r t_r + 1)(E_r t_r + 1)}, \quad \text{(Equation 2)}$$

where f_{bi} is the resonance frequency of the bilayer beam, E_r is the Young's modulus ratio E_f/E_s, t_r is the thickness ratio t_f/t_s, ρ_r is the density ratio ρ_f/ρ_s, and the subscripts f and s correspond to the thin film and main substrate, respectively. For $t_r \ll 1$ and small E_r and ρ_r values, Equation 2 can be further reduced to

$$E_{LPGA} = \frac{1}{3} E_s \cdot \left(\frac{2\Delta f}{t_r f_s} + \rho_r\right), \quad \text{(Equation 3)}$$

where $\Delta f = f_{bi} - f_s$ is the frequency shift. For the LPGA density, the value ρ_{LPGA} = 1,444 kg m^{-3} was used.[43] An average value of the Young's modulus of the LPGA thin film E_{LPGA} = 1.52 GPa was calculated. It is important to note that the Young's modulus of LPGA in the form of a thin crystalline film appears to be notably different from the values obtained using nanoindentation (2.3–3.9 GPa) on single crystals,[43] even though elasticity is an intrinsic property and hence the values should be identical. However, given the polycrystalline nature of the deposited LPGA thin film and that the Young's modulus measured by monitoring shifts in resonance frequency is reflective of the bulk modulus compared with the surface-specific indentation modulus, the substantial difference observed is not unexpected.

After optimizing the thermal evaporation parameters, we deposited LPGA on MC-As (see Figure S1B; supplemental information) to fabricate the hybrid TS-OC-MEMS device. Resonance frequency measurements were conducted on eight identical TS-OC-MEMS devices, and the mean frequency shift between LPGA-free and LPGA-charged MC-A cantilevers was Δf = 270 Hz (Figure 2B). Given the multilayered structure (Si–SiO_2–Au wires–LPGA) and the irregular shape of the cross-section, an ANSYS model was used to determine the Young's modulus of the LPGA thin film (see Figure S4; supplemental information). The result (≈1 GPa) matches the value determined from the resonance frequency measurement on the LPGA-charged MC-P cantilever (1.52 GPa).

To evaluate the LPGA $\alpha \rightarrow \beta$ phase transition, we subjected LPGA-free and LPGA-charged MC-A cantilevers to temperature ramps between 30°C and 100°C at a heating/cooling rate of 10°C min^{-1} over two cycles. The variation of the resonance frequency as a function of temperature in the case of LPGA-free MC-A is illustrated in Figure 2C. For each cycle, the slope m reflecting the change in resonant frequency with respect to temperature on heating and cooling was determined using linear regressions and averaged at $m_{H,avg} = -0.796 \pm 0.004$ and $m_{L,avg} = -0.792 \pm 0.001$. At $T \neq T_{ambient}$, for moment of inertia $I = \frac{w \cdot t^3}{12}$ and cross-sectional surface area $A = w \cdot t$, Equation 1 becomes

$$f(T) = \frac{0.56}{\sqrt{12}} \cdot \frac{t_i + t_i \cdot \Delta T \cdot \alpha(T)}{(L_i + L_i \cdot \Delta T \cdot \alpha(T))^2} \cdot \sqrt{\frac{E(T)}{\rho(T)}}, \quad \text{(Equation 4)}$$

where the major contributor to the change in resonant frequency is the dependence of silicon's Young's modulus on temperature (−60 ppm $°C^{-1}$). However, the stiffness of the structure is also affected by any dimensional changes in length, width, or thickness, which subsequently changes the resonant frequency. In LPGA-charged MC-A

Please cite this article in press as: Mahmoud Halabi et al., Microelectromechanical devices driven by thermosalient effects, Cell Reports Physical Science (2022), https://doi.org/10.1016/j.xcrp.2022.101133

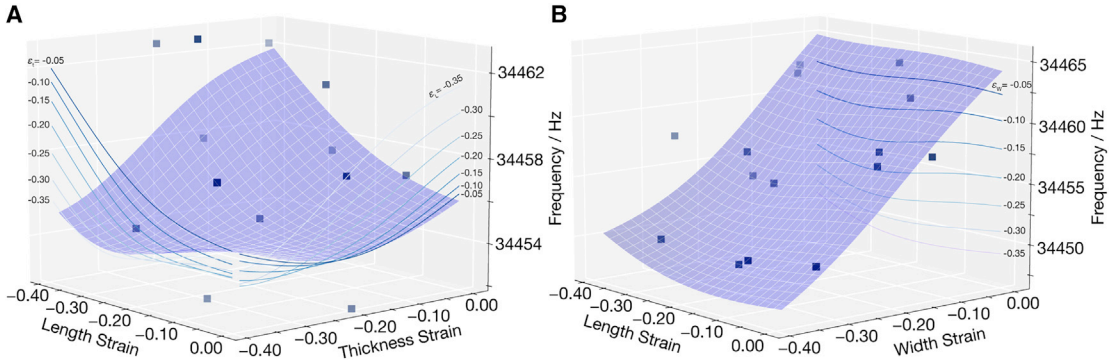

Figure 3. Simulated resonance frequency versus three-dimensional (3D) strain surface plots

(A and B) Change of LPGA-charged cantilever's resonance frequency at 100°C with respect to strain along the length, width, and thickness of the LPGA thin film as a result of phase transition. The scatter points are the design points used to construct the surface plots, and the contour lines are two-dimensional slices of the 3D surface projected along ϵ_L, ϵ_W, or ϵ_t.

cantilevers, LPGA undergoes anisotropic expansion during the phase transition. Therefore, studying the change in resonant frequency of the LPGA-charged MC-A cantilevers as the LPGA film undergoes phase transition helps quantify the induced strain along the length, width, and thickness of the thin film $(\epsilon_L, \epsilon_W, \epsilon_t)$.

Across all eight tested LPGA-charged MC-A cantilevers, the variation of the resonance frequency with temperature shows a hysteresis, as illustrated in Figure 2D. This hysteresis is a signature of the LPGA $\alpha \rightarrow \beta$ phase transition on heating with a slope change in the curve *f:* $T_i \rightarrow T_f$ around 80°C from $m_{H,avg-\alpha} = -0.981 \pm 0.01$ before the phase transition to $m_{H,avg-\beta} = -1.418 \pm 0.041$ after the phase transition. The inflection points were determined by monitoring the change in the sign of the second derivative. The $\beta \rightarrow \alpha$ phase transition is also visible on cooling around 70°C with a slope change in the curve *f:* $T_f \rightarrow T_i$ from $m_{L,avg-\beta} = -1.246 \pm 0.019$ before the phase transition to $m_{L,avg-\alpha} = -0.972 \pm 0.002$. Any change in resonance frequency is dependent on the change in mass or stiffness of the beam. Given that the same behavior is reproducible over multiple cycles, we can safely assume that there is no loss in mass of the LPGA film throughout the phase transition. Therefore, the hysteresis shown corresponds to a change in the stiffness of the microcantilever because of the induced compression strain in the LPGA film, proving the phase transition in the thin-film form is reversible and preserved.

ANSYS simulation of LPGA-charged MC-A cantilever

The deposited LPGA thin film in the TS-OC-MEMS device was shown to be polycrystalline. As a result, information on the strain along the length, width, or thickness of the deposited film cannot be directly related to the X-ray diffraction information on the crystal lattice strain induced by the phase transition in LPGA single crystals. Additionally, the defined lattice parameters in the single crystal form can align constructively or destructively in the polycrystalline thin film, thereby preventing a clear correlation between the thin-film and single-crystal behavior. Therefore, to determine the strain induced in the LPGA film because of the phase transition, we simulated the LPGA-charged MC-A cantilever using a static structural model in ANSYS paired with a modal analysis to determine the resonant frequency change (see Figure S4; supplemental information). The three-dimensional surface plot in Figure 3 explains the variation of the resonant frequency of the microcantilever with respect to strain along the length, width, and thickness (Figures 3A and 3B) of the LPGA thin film at $T_f = 100$°C. The resonant frequency of the LPGA-charged cantilever was determined

Please cite this article in press as: Mahmoud Halabi et al., Microelectromechanical devices driven by thermosalient effects, Cell Reports Physical Science (2022), https://doi.org/10.1016/j.xcrp.2022.101133

from the simulation to be $f_{OC-MEMS}$ = 34.521 kHz at T = 30°C with a 7.4% error compared with the resonant frequency obtained from dynamic frequency measurements ($f_{OC-MEMS}$ = 32.121 kHz) at the same temperature (Figure 2B; see experimental procedures). The surface plots were then optimized over two stages to narrow down the dimensional strain combinations in the LPGA thin film that could lead to the same shift recorded in the dynamic frequency measurements.

First, boundary conditions were applied to the dimensional strains such that $-0.51 \leq \epsilon_{(x,y,z)} \leq 0$ and the volumetric strain $\epsilon_V = \epsilon_x + \epsilon_y + \epsilon_z \leq -0.665$.[41] The combinations of strains along the length, width, and thickness of the LPGA film that fall within the specified boundary conditions and yield a drop in resonant frequency equal to that observed experimentally at T_f ($\Delta f \approx 75$ Hz) were extracted. Note that up to this point the extracted strain combinations are based only on the change between the initial resonant frequency of the TS-OC-MEMS device at T_i and the resonant frequency at the final temperature after heating. In the second stage, the candidate strain combinations obtained were plugged back into the simulation model, and the change in frequency and maximum deformation of the cantilever tip were monitored in real time with respect to the change in temperature.

Figure 4A shows the parameter sensitivities used to determine to what extent the variables of interest (frequency and deformation) are affected by a change in any of the considered optimization parameters (dimensional strain and temperature). The change of frequency and maximum deformation with respect to temperature is shown in Figures 4B and 4C at different strains along the width and length of the LPGA film, respectively, while controlling the strain along the other dimensions. The same simulation was rerun with different optimized strain combinations obtained in the first stage, and the slope of the decreasing resonant frequency with respect to temperature was determined for each simulation. These slopes were then compared with the average slope obtained experimentally (Figure 2D). This step ensured that the optimization process is based not only on the final actuated state but also on the dynamic behavior of the cantilever throughout the actuation to avoid exaggerated linearity assumptions. The optimal simulation strain parameters that best mimic the real behavior of the TS-OC-MEMS cantilever were determined accordingly. Note that because it was not possible to trigger a sudden phase transition at a specific temperature in the ANSYS simulation, the phase transition strain was introduced through a thermal coefficient. Hence inflection points similar to those observed experimentally are not visible here, and the effect was averaged out over the entire range of temperatures instead.

The three-dimensional strain induced by the phase transition in the deposited LPGA polycrystalline thin film was estimated along the length, width, and thickness ($\epsilon_L = -0.12 \pm 0.05$, $\epsilon_W = -0.28 \pm 0.01$, $\epsilon_t = -0.14 \pm 0.05$). The resultant maximum tip deformation is δ_{max} = 3.91 μm. The stark anisotropic effects observed in the LPGA single-crystal form as a result of the phase transition are more averaged out in the thin film form, given the polycrystalline nature of the latter and the random orientation of the crystalline domains with respect to the dimensions of the cantilever where the film is deposited. For the same reason, the maximum mechanical strain induced by the phase transition in the LPGA thin film is lower than the LPGA lattice strain but remains at least 10 times larger than the mechanical strain induced in the single crystal form (~1.75%). As expected, the thin film form allowed for a smoother dissipation of the elastic energy within the structure where the accumulated stresses are diffused through mechanical contraction instead of crack formation, which also helps preserve the integrity of the structure. It is likely that increasing the surface-area-to-volume ratio promoted a more

Please cite this article in press as: Mahmoud Halabi et al., Microelectromechanical devices driven by thermosalient effects, Cell Reports Physical Science (2022), https://doi.org/10.1016/j.xcrp.2022.101133

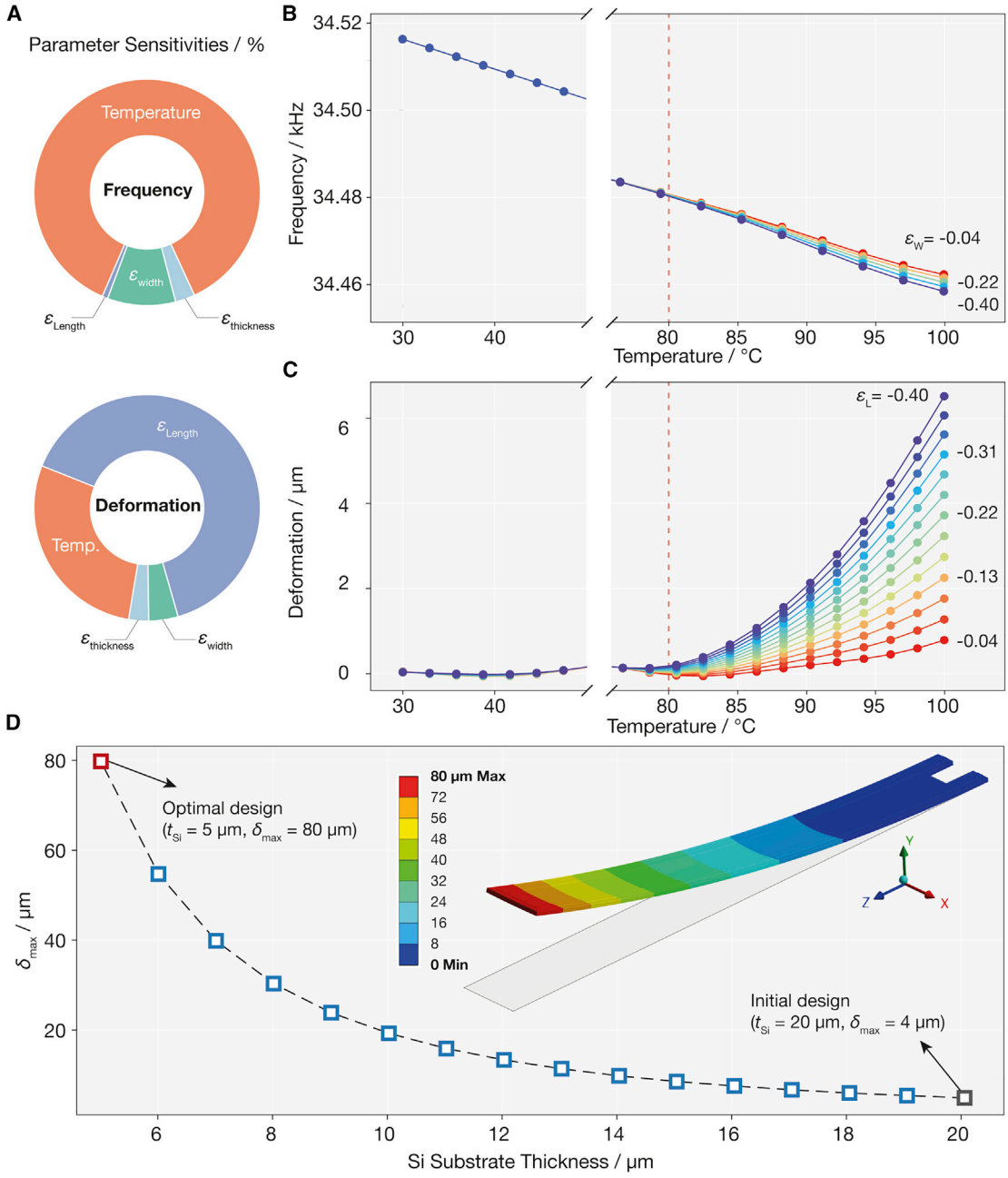

Figure 4. Frequency and deformation dependence on dimensional LPGA strain variables and temperature and design optimization

(A) Sensitivity of frequency and deformation of the TS-OC-MEMS device to temperature and three-dimensional strain in the LPGA thin film.

(B) The change of the cantilever's frequency with respect to temperature at different strain rates along the thin film's width.

(C) The change of the cantilever's tip deformation with respect to temperature at different strain rates along the thin film's length.

(D) The change of maximum deformation in LPGA-charged MC-A cantilever as a function of silicon substrate thickness.

stable molecular reconfiguration and aided the reformation of the robust network of intermolecular interactions that exist in the LPGA structure.[41] Subjecting the cantilever to a few actuation cycles showed consistent behavior, reflecting the structural stability and preservation of the phase transition characteristics of the LPGA film. However, further cyclic testing is required to confirm the durability of the thin film over 100 actuation cycles.

Please cite this article in press as: Mahmoud Halabi et al., Microelectromechanical devices driven by thermosalient effects, Cell Reports Physical Science (2022), https://doi.org/10.1016/j.xcrp.2022.101133

The resultant deformation appears to be minimal; however, we note that the cantilever design tested here is not geometrically optimized to yield the maximum response possible. The main silicon substrate has a substantial thickness and contributes significantly to the stiffness of the cantilever, thereby decreasing the maximum possible deformation. The thickness of the silicon substrate was optimized for maximum tip deflection, and a range of thicknesses between 5 and 20 μm were considered within an acceptable range of manufacturing limitations. The maximum deflection δ_{max} was recorded for each simulated design and plotted in Figure 4D with respect to the thickness of the silicon layer t_{Si}. The deflection increases rapidly for t_{Si} < 10 μm. A thickness t_{Si} = 5 μm yields optimal maximum deflection δ_{max} = 80 μm. The maximum deflection undergoes a 20-fold increase with only a 75% decrease in silicon thickness.

Research on dynamic molecular crystals has demonstrated the unique properties of these structures. Their long-range order is invaluable because it allows for accurate mapping of the molecular configuration in the entire crystal through simple diffraction methods. Assuming such homogeneity and uniformity in materials properties across the entire crystal structure also contributes to increased accuracy in modeling. Such properties are not available in amorphous soft polymeric actuators, which stands as one of the major setbacks in simulating and controlling their behavior. However, with the excessive focus on single-material structures and crystalline materials for easier modeling and more efficient energy transduction, comparatively little exploration has gone into pairing molecular crystals with other compatible materials to integrate them into devices.

To circumvent the limitations in synthesis and geometric flexibility due to complex and, in many cases, unpredictable crystallization processes, here we explored the preparation of LPGA polycrystalline thin films through thermal evaporation, allowing for increased modulation of the film's properties. The process was optimized to reduce polycrystalline growth, ensure continuity, and control the thickness of the thin film that was integrated into a MEMS device to further characterize its mechanical properties and dynamic response. We found that the phase transition of LPGA, considered unique to the single crystal form, is preserved in the thin film, and therefore the film was introduced as an active actuating material that drives tip deflection in the TS-OC-MEMS cantilever with temperature change over the phase transition temperature. Further, using finite element analysis, the LPGA-charged MEMS device was simulated to extract information on the induced mechanical strain in the thin film and to optimize the geometric design of the cantilever aimed at increasing the amplitude of actuation. The phase transition in LPGA has been reported to be faster than in other thermosalient compounds, spin-crossover compounds, and other single-crystal-to-single-crystal transitions.[36] The rapid response of phase transitions offers a much faster actuation time (~4 ms) than typical shape memory (~2.7 s)[44] and bimetallic thermal actuators (0.04–127 s)[44] that are limited by the heat capacity and coefficients of thermal expansion (CTEs) of the material. This work offers a new direction that maximizes the utility of dynamic molecular crystals in mechanically robust devices and applications and ensures reproducibility in fabrication and utilization of these crystals as actuating elements. A recent review on energy-harvesting devices highlights the promising yet studied potential of pyroelectric effects (generation of voltage from a temperature fluctuation) in energy harvesting, sensing, and storage applications and flexible devices.[45] Pairing thermosalient organic crystals and piezoelectric materials yields a rapid, CTE-independent, pyroelectric response. Hybrid TS-OC-MEMS devices bring about an opportunity to experiment with new materials in MEMSs research and have the potential to reinvigorate the currently

Please cite this article in press as: Mahmoud Halabi et al., Microelectromechanical devices driven by thermosalient effects, Cell Reports Physical Science (2022), https://doi.org/10.1016/j.xcrp.2022.101133

declining interest in the field. The growing library of responsive molecular crystals with a variety of unique properties promises many potential candidates that can be investigated for more compatible pairing with MEMSs toward advanced actuation and sensing capabilities.

EXPERIMENTAL PROCEDURES

Resource availability

Lead contact

Further information requests should be directed to and will be fulfilled by the lead contact, Panče Naumov (pance.naumov@nyu.edu).

Materials availability

This study did not generate new unique reagents.

Data and code availability

All data are available in the main text or the supplemental information.

Preparation of the LPGA films

LPGA was chosen as the ideal candidate for evaporation experiments based on previous experiments, actuation behavior, cyclability, molecular weights, melting points, and phase transition temperatures. Before their integration in MEMS devices, thin films of LPGA were first prepared on silicon wafers to study their morphological and structural properties. Before the LPGA deposition, silicon substrates were thoroughly cleaned with acetone and isopropanol and treated with an oxygen plasma. Organic films were then made by LPGA sublimation at 65°C under high vacuum (2×10^{-7} mbar) at a low growth rate of 0.7 Å s^{-1}. The thickness of the films and the deposition flux were controlled by a quartz crystal microbalance (QCM) placed near the sample located 30 cm above the effusion cell. According to the QCM, the estimated thicknesses of 50, 100, 150, and 600 nm of LPGA were deposited onto the substrates. It should be noted here that immediately after removing the samples from the vacuum chamber, a noticeable reorganization of the deposited thin films occurred over time, regardless of the LPGA thickness. For the thickest estimated layers, those morphological modifications led to reproducible and stable films, whereas they induced discontinuous films for thicknesses under 100 nm of evaporated LPGA. In addition, we confirmed that the substrate surface preparation (with or without oxygen plasma treatment) revealed no differences in the post-deposition behavior of LPGA. One possible hypothesis for this observation is that the origin of the morphological changes in this material (just after exposure to nitrogen or air) could be because of intrachain hydrogen bonding present in the LPGA structure.[40,46] Optical microscopy of the 600-nm-thick LPGA layer shows large domains (on the order of tens of μm^2) generated by this reorganization process. For their implementation on MC-A cantilevers, thickness of the LPGA layer of 600 nm was deemed the most suitable to obtain a continuous thin film, given that the top surface of the cantilever is not entirely flat due to the deposited gold wire.

Microcantilever device fabrication

Two types of microcantilever device were fabricated: MC-Ps composed of bare silicon and MC-As with integrated actuation and detection capabilities. The MC-P device has an array of eight silicon cantilevers 500 μm in length, 100 μm in width, and 5 μm in thickness fabricated from a silicon-on-insulator (SOI) 100 n-type substrate. The fabrication process includes front-side lithography followed by reactive ion etching (RIE) of the silicon to define the geometry of the cantilevers and then

Please cite this article in press as: Mahmoud Halabi et al., Microelectromechanical devices driven by thermosalient effects, Cell Reports Physical Science (2022), https://doi.org/10.1016/j.xcrp.2022.101133

back-side lithography followed by a deep RIE (DRIE) step to release the cantilevers (see Figure S1A; supplemental information). MC-A chips consist of silicon-based microcantilevers with integrated electromagnetic actuation and piezoresistive sensing schemes used in measuring the hydrodynamic forces and rheological properties of fluids.[47] These cantilevers can be precisely fabricated through anisotropic etching and local oxidation using masking layers to create different designs.[48] The MC-A chip includes a measure cantilever (840-μm-long, 100-μm-wide, and 20-μm-thick silicon base) and an unreleased reference cantilever with similar geometry (see Figure S1B; supplemental information).

AFM

To measure the thickness of the LPGA films, we used AFM (Bruker Dimension Icon). During the deposition of LPGA film by evaporation, one part of the wafer was covered to block any LPGA deposition. In AFM imaging, the boundary between the LPGA-free area and the deposited LPGA film was scanned to measure the thickness. Tapping mode was used with a cantilever Bruker RTESP model while scanning. The frequency of the cantilever for the tapping mode was 397 kHz. Figure S2 (see supplemental information) shows the AFM topography with height sensor mode after software-assisted compensation of tilting (using NanoScope Analysis of Bruker Corporation). The left part of Figure S2 is the LPGA-free area, and the right part is the deposited LPGA. The scanning range was 20 × 20 μm, and the scanning rate was 0.53 Hz. The cross-sectional topography shows that the average thickness of the LPGA film was about 552 nm.

Crystallographic analysis

Crystallographic analysis of LPGA films was performed with a Bruker D8 Advance diffractometer used in grazing incidence mode at room temperature. The device is equipped with a copper anti-cathode (λ Cu $K_{\alpha 1}$ = 1.54056 Å and λ Cu $K_{\alpha 2}$ = 1.54443 Å), and a Bruker LynxEye detector configured in 0 D mode opened at 10 mm. The sample is positioned on a motorized XYZ stage. The incidence angle was fixed at 1°, and the acquisitions were made in an angular range from 15° to 50° in 2θ, with a measurement step of 0.016° and time steps of 5 s. For the variable-temperature diffraction measurements, the sample was placed in an Anton Paar HTK1200N chamber and heated up to 100°C with a ramp of 2°C. The diffractograms (XRD patterns) were recorded every 10°C. A stabilization time of 5 min was allowed before each recording made between 18.5° and 27.5° in 2θ, with a measurement step of 0.02° and a time in steps of 4 s. The crystalline phases were identified using the software DiffracPlus EVA[49] combined with the ICDD-Powder Diffraction File database (PDF, #00-037-1706).

Dynamic frequency measurements

The dynamic measurements were carried out in an HFS350V (Linkam Scientific) stage. A piezoelectric disc (PRYY-1077) from Physik Instrumente was used to vibrate the cantilevers in the MC-P device. A confocal displacement sensor (IFS2407-3 from Micro-Epsilon) was used to detect the resonance frequency. In the case of the MC-A device, a magnet was placed inside the Linkam stage to generate the Lorentz force necessary to vibrate the cantilevers. The force results from the magnetic field and the alternating electric current (500 μA) that runs through the metallic excitation wire in each cantilever. The resonance frequency is measured by monitoring the change in the piezoresistance value of the unrestrained cantilever. All measurements and acquisitions were carried out using a dedicated home-made electronic setup already described in an article by Alava et al.[50]

ANSYS simulation of LPGA-charged cantilever

A static structural model was used to simulate the bending behavior of the LPGA-charged MEMS cantilever in ANSYS (see Figure S4; supplemental information). The cantilever is composed of a 20-μm-thick main pure-silicon layer, a 0.5-μm silicon dioxide layer, a gold conductive layer of 0.6 μm in thickness and 10 μm in width that circulates the cantilever at 10 μm from the edges, and a final layer of LPGA of 0.6 μm in thickness.

It is important to note that the gold and LPGA layers are estimated at a uniform thickness even though, in reality, they are not as uniformly layered, and therefore differences between simulation and experimental results are expected and inevitable. The entire structure was then discretized by using a mesh control that sweeps each body through its thickness where there are at least two elements through each layer. A quadrilateral mesh suitable for bending was used with an optimized element size suitable for each body. The mechanical and physical properties, such as the Young's modulus, density, and thermal expansion coefficients, were assigned for each layer in tabular form at different temperatures. The LPGA layer was assigned a Young's modulus of 1.52 GPa determined experimentally through resonance frequency experiments and an estimated Poisson's ratio $\nu = 0.3$.

To simulate the thermally induced phase transition in LPGA, we assigned a range of thermal coefficients $-0.0065°C^{-1} \leq \alpha_{LPGA} \leq 0°C^{-1}$ in each direction based on the X-ray diffraction data obtained on the phase transition in the single-crystal LPGA form and the temperature range of $\Delta T = 78°C^{-1}$. A fixed support was applied to one end of the cantilever where it is clamped, and a thermal condition was introduced as a temperature increase from room temperature $T_i = 22°C$ to $T_f = 100°C$. The resonance frequency of the entire structure along the bending axis was measured before and after bending.

SUPPLEMENTAL INFORMATION

Supplemental information can be found online at https://doi.org/10.1016/j.xcrp.2022.101133.

ACKNOWLEDGMENTS

This research was partially performed by using the Core Technology Platform (CTP) resources at New York University Abu Dhabi and partly supported by the French Renatech network and the NYU GSAS Horizon Fellowship.

AUTHOR CONTRIBUTIONS

Conceptualization, J.M.H., L.N., and P.N.; methodology, J.M.H., I.S., F.M., B.D., L.N., D.P.K., and P.N.; investigation, J.M.H., I.S., L.S., T.L., D.S., F.M., B.P., L.N., and P.N.; writing – original draft, J.M.H., L.N., and P.N.; writing – review & editing, J.M.H., L.N., and P.N.; supervision, L.N. and P.N.

DECLARATION OF INTERESTS

The authors declare no competing interests.

Received: August 1, 2022
Revised: September 19, 2022
Accepted: October 13, 2022
Published: November 4, 2022

REFERENCES

1. Kim, T., Zhu, L., Al-Kaysi, R.O., and Bardeen, C.J. (2014). Organic photomechanical materials. ChemPhysChem *15*, 400–414. https://doi.org/10.1002/cphc.201300906.
2. Koshima, H., Matsuo, R., Matsudomi, M., Uemura, Y., and Shiro, M. (2013). Light-driven bending crystals of salicylidenephenylethylamines in enantiomeric and racemate forms. Cryst. Growth Des. *13*, 4330–4337. https://doi.org/10.1021/cg400675r.
3. Zhu, L., Al-Kaysi, R.O., and Bardeen, C.J. (2016). Photoinduced ratchet-like rotational motion of branched molecular crystals. Angew. Chem. Int. Ed. *55*, 7073–7076. https://doi.org/10.1002/anie.201511444.
4. Karothu, D.P., Dushaq, G., Ahmed, E., Catalano, L., Polavaram, S., Ferreira, R., Li, L., Mohamed, S., Rasras, M., and Naumov, P. (2021). Mechanically robust amino acid crystals as fiber-optic transducers and wide bandpass filters for optical communication in the near-infrared. Nat. Commun. *12*, 1326. https://doi.org/10.1038/s41467-021-21324-y.
5. Mahmoud Halabi, J., Ahmed, E., Catalano, L., Karothu, D.P., Rezgui, R., and Naumov, P. (2019). Spatial photocontrol of the optical output from an organic crystal waveguide. J. Am. Chem. Soc. *141*, 14966–14970. https://doi.org/10.1021/jacs.9b07645.
6. Annadhasan, M., Agrawal, A.R., Bhunia, S., Pradeep, V.V., Zade, S.S., Reddy, C.M., and Chandrasekar, R. (2020). Mechanophotonics: flexible single-crystal organic waveguides and circuits. Angew. Chem. Int. Ed. *59*, 13852–13858. https://doi.org/10.1002/anie.202003820.
7. Catalano, L., Berthaud, J., Dushaq, G., Karothu, D.P., Rezgui, R., Rasras, M., Ferlay, S., Hosseini, M.W., and Naumov, P. (2020). Sequencing and welding of molecular single-crystal optical waveguides. Adv. Funct. Mater. *30*, 2003443. https://doi.org/10.1002/adfm.202003443.
8. Catalano, L., Karothu, D.P., Schramm, S., Ahmed, E., Rezgui, R., Barber, T.J., Famulari, A., and Naumov, P. (2018). Dual-mode light transduction through a plastically bendable organic crystal as an optical waveguide. Angew. Chem. Int. Ed. *57*, 17254–17258. https://doi.org/10.1002/anie.201810514.
9. Jiang, H., and Hu, W. (2020). The emergence of organic single-crystal electronics. Angew. Chem. Int. Ed. *59*, 1408–1428. https://doi.org/10.1002/anie.201814439.
10. Huang, R., Wang, C., Wang, Y., and Zhang, H. (2018). Elastic self-doping organic single crystals exhibiting flexible optical waveguide and amplified spontaneous emission. Adv. Mater. *30*, 1800814. https://doi.org/10.1002/adma.201800814.
11. Chandrasekar, R. (2014). Organic photonics: prospective nano/micro scale passive organic optical waveguides obtained from π-conjugated ligand molecules. Phys. Chem. Chem. Phys. *16*, 7173–7183. https://doi.org/10.1039/C3CP54994A.
12. Han, D.D., Zhang, Y.L., Ma, J.N., Liu, Y.Q., Han, B., and Sun, H.B. (2016). Light-mediated manufacture and manipulation of actuators. Adv. Mater. *28*, 8328–8343. https://doi.org/10.1002/adma.201602211.
13. Tang, Q., Tong, Y., Hu, W., Wan, Q., and Bjørnholm, T. (2009). Assembly of nanoscale organic single-crystal cross-wire circuits. Adv. Mater. *21*, 4234–4237. https://doi.org/10.1002/adma.200901355.
14. Wang, X.L., Xue, J.P., Sun, X.P., Zhao, Y.X., Wu, S.Q., Yao, Z.S., and Tao, J. (2020). Giant single-crystal shape transformation with wide thermal hysteresis actuated by synergistic motions of molecular cations and anions. Chem. Eur. J. *26*, 6778–6783. https://doi.org/10.1002/chem.202000845.
15. Hulea, I.N., Fratini, S., Xie, H., Mulder, C.L., Iossad, N.N., Rastelli, G., Ciuchi, S., and Morpurgo, A.F. (2006). Tunable Fröhlich polarons in organic single-crystal transistors. Nat. Mater. *5*, 982–986. https://doi.org/10.1038/nmat1774.
16. Tang, Q., Li, H., Liu, Y., and Hu, W. (2006). High-performance air-stable n-type transistors with an asymmetrical device configuration based on organic single-crystalline submicrometer/nanometer ribbons. J. Am. Chem. Soc. *128*, 14634–14639. https://doi.org/10.1021/ja064476f.
17. Ding, R., Feng, J., Zhou, W., Zhang, X.L., Fang, H.H., Yang, T., Wang, H.Y., Hotta, S., and Sun, H.B. (2015). Intrinsic polarization and tunable color of electroluminescence from organic single crystal-based light-emitting devices. Sci. Rep. *5*, 12445. https://doi.org/10.1038/srep12445.
18. Tang, K., Song, Z., Tang, Q., Tian, H., Tong, Y., and Liu, Y. (2018). Effect of the deformation state on the response of a flexible H 2 S sensor based on a Ph5T2 single-crystal transistor. IEEE Electron. Device Lett. *39*, 119–122. https://doi.org/10.1109/LED.2017.2770181.
19. Fraboni, B., Fraleoni-Morgera, A., and Zaitseva, N. (2016). Ionizing radiation detectors based on solution-grown organic single crystals. Adv. Funct. Mater. *26*, 2276–2291. https://doi.org/10.1002/adfm.201502669.
20. Deng, W., Zhang, X., Jia, R., Huang, L., Zhang, X., and Jie, J. (2019). Organic molecular crystal-based photosynaptic devices for an artificial visual-perception system. NPG Asia Mater. *11*, 77. https://doi.org/10.1038/s41427-019-0182-2.
21. Landi, A., Peluso, A., and Troisi, A. (2021). Quantitative prediction of the electro-mechanical response in organic crystals. Adv. Mater. *33*, 2008049. https://doi.org/10.1002/adma.202008049.
22. Choi, H.H., Yi, H.T., Tsurumi, J., Kim, J.J., Briseno, A.L., Watanabe, S., Takeya, J., Cho, K., and Podzorov, V. (2020). A large anisotropic enhancement of the charge carrier mobility of flexible organic transistors with strain: a Hall effect and Raman study. Adv. Sci. *7*, 1901824. https://doi.org/10.1002/advs.201901824.
23. Seki, T., Sakurada, K., Muromoto, M., and Ito, H. (2015). Photoinduced single-crystal-to-single-crystal phase transition and photosalient effect of a gold (I) isocyanide complex with shortening of intermolecular aurophilic bonds. Chem. Sci. *6*, 1491–1497. https://doi.org/10.1039/C4SC02676D.
24. Panda, M.K., Runčevski, T., Sahoo, S.C., Belik, A.A., Nath, N.K., Dinnebier, R.E., and Naumov, P. (2014). Colossal positive and negative thermal expansion and thermosalient effect in a pentamorphic organometallic martensite. Nat. Commun. *5*, 4811. https://doi.org/10.1038/ncomms5811.
25. Mittapalli, S., Sravanakumar Perumalla, D., and Nangia, A. (2017). Mechanochemical synthesis of N-salicylideneaniline: thermosalient effect of polymorphic crystals. IUCrJ *4*, 243–250. https://doi.org/10.1107/S2052252517004043.
26. Mittapalli, S., Perumalla, D.S., Nanubolu, J.B., and Nangia, A. (2017). Thermomechanical effect in molecular crystals: the role of halogen-bonding interactions. IUCrJ *4*, 812–823. https://doi.org/10.1107/S2052252517014658.
27. So, H.S., Minami, T., Jindo, T., and Matsumoto, S. (2018). Thermosalient effect of two polymorphs of a diketopyrrolopyrrole dye with different crystal systems and molecular arrangements. CrystEngComm *20*, 5317–5320. https://doi.org/10.1039/C8CE00940F.
28. Commins, P., Natarajan, A., Tsai, C.K., Khan, S.I., Nath, N.K., Naumov, P., and Garcia-Garibay, M.A. (2015). Structure–reactivity correlations and mechanistic understanding of the photorearrangement and photosalient effect of α-santonin and its derivatives in solutions, crystals, and nanocrystalline suspensions. Cryst. Growth Des. *15*, 1983–1990. https://doi.org/10.1021/acs.cgd.5b00135.
29. Takeda, T., Ozawa, M., and Akutagawa, T. (2019). Jumping crystal of a hydrogen-bonded organic framework induced by the collective molecular motion of a twisted π system. Angew. Chem. Int. Ed. *58*, 10345–10352. https://doi.org/10.1002/ange.201905075.
30. Kitagawa, D., Okuyama, T., Tanaka, R., and Kobatake, S. (2016). Photoinduced rapid and explosive fragmentation of diarylethene crystals having urethane bonding. Chem. Mater. *28*, 4889–4892. https://doi.org/10.1021/acs.chemmater.6b02017.
31. Yadava, K., and Vittal, J.J. (2019). Photosalient behavior of photoreactive Zn (II) complexes. Cryst. Growth Des. *19*, 2542–2547. https://doi.org/10.1021/acs.cgd.9b00260.
32. Naumov, P., Karothu, D.P., Ahmed, E., Catalano, L., Commins, P., Mahmoud Halabi, J., Al-Handawi, M.B., and Li, L. (2020). The rise of the dynamic crystals. J. Am. Chem. Soc. *142*, 13256–13272. https://doi.org/10.1021/jacs.0c05440.
33. Panda, M.K., Etter, M., Dinnebier, R.E., and Naumov, P. (2017). Acoustic emission from organic martensites. Angew. Chem. Int. Ed. Engl. *56*, 8104–8109. https://doi.org/10.1002/anie.201702359.
34. Park, S.K., and Diao, Y. (2020). Martensitic transition in molecular crystals for dynamic functional materials. Chem. Soc. Rev. *49*, 8287–8314. https://doi.org/10.1039/D0CS00638F.

35. Zakharov, B.A., Michalchuk, A.A.L., Morrison, C.A., and Boldyreva, E.V. (2018). Anisotropic lattice softening near the structural phase transition in the thermosalient crystal 1, 2, 4, 5-tetrabromobenzene. Phys. Chem. Chem. Phys. *20*, 8523–8532. https://doi.org/10.1039/C7CP08609A.

36. Ahmed, E., Karothu, D.P., Slimani, A., Mahmoud Halabi, J., Tahir, I., Canales, K.Q., and Naumov, P. (2022). Ultrafast, light, soft martensitic materials. Adv. Funct. Mater. *32*, 2112117. https://doi.org/10.1002/adfm.202112117.

37. Leïchlé, T., Nicu, L., and Alava, T. (2020). MEMS biosensors and COVID-19: missed opportunity. ACS Sens. *5*, 3297–3305. https://doi.org/10.1021/acssensors.0c01463.

38. Ayela, C., Vandevelde, F., Lagrange, D., Haupt, K., and Nicu, L. (2007). Combining resonant piezoelectric micromembranes with molecularly imprinted polymers. Angew. Chem. Int. Ed. *46*, 9271–9274. https://doi.org/10.1002/anie.200703881.

39. Dezest, D., Leïchlé, T., Teerapanich, P., Mathieu, F., Bui, B.T.S., Haupt, K., and Nicu, L. (2019). Multiplexed functionalization of nanoelectromechanical systems with photopatterned molecularly imprinted polymers. J. Micromech. Microeng. *29*, 025013. https://doi.org/10.1088/1361-6439/aaf84e.

40. Wu, H., Reeves-McLaren, N., Pokorny, J., Yarwood, J., and West, A.R. (2010). Polymorphism, phase transitions, and thermal stability of L-pyroglutamic acid. Cryst. Growth Des. *10*, 3141–3148. https://doi.org/10.1021/cg100260f.

41. Panda, M.K., Runčevski, T., Husain, A., Dinnebier, R.E., and Naumov, P. (2015). Perpetually self-propelling chiral single crystals. J. Am. Chem. Soc. *137*, 1895–1902. https://doi.org/10.1021/ja5111927.

42. Whiting, R., Angadi, M.A., and Tripathi, S. (1995). Evaluation of elastic moduli in thin-film/substrate systems by the two-layer vibrating reed method. Mater. Sci. Eng., B *30*, 35–38. https://doi.org/10.1016/0921-5107(94)01133-8.

43. Karothu, D.P., Mahmoud Halabi, J., Li, L., Colin-Molina, A., Rodríguez-Molina, B., and Naumov, P. (2020). Global performance indices for dynamic crystals as organic thermal actuators. Adv. Mater. *32*, 1906216. https://doi.org/10.1002/adma.201906216.

44. Ansys GRANTA EduPack Software, ANSYS, Inc., Cambridge, UK, 2022 (www.ansys.com/materials).

45. Vijayakanth, T., Liptrot, D.J., Gazit, E., Boomishankar, R., and Bowen, C.R. (2022). Recent advances in organic and organic–inorganic hybrid materials for piezoelectric mechanical energy harvesting. Adv. Funct. Mater. *32*, 2109492. https://doi.org/10.1002/adfm.202109492.

46. Van Zoeren, E., Oonk, H.A.J., and Kroon, J. (1978). X-ray analysis of l-pyroglutamic acid. A marked case of structural pseudosymmetry. Acta Crystallogr. Sect. B *34*, 1898–1900. https://doi.org/10.1107/S0567740878006925.

47. Dufour, I., Maali, A., Amarouchene, Y., Ayela, C., Caillard, B., Darwiche, A., Guirardel, M., Kellay, H., Lemaire, E., Mathieu, F., et al. (2012). The microcantilever: a versatile tool for measuring the rheological properties of complex fluids. J. Sens. *2012*, 1–9. https://doi.org/10.1155/2012/719898.

48. Saya, D., Leïchlé, T., Pourciel, J.B., Mathieu, F., Bergaud, C., and Nicu, L. (2008). Contact force control of piezoresistive cantilevers with in-plane nanotips for femtoliter droplet deposition. Microelectron. Eng. *85*, 1341–1345. https://doi.org/10.1016/j.mee.2007.12.066.

49. DIFFRACplus EVA Version 13.0, Bruker AXS, Inc., Madison, WI, USA, 2007.

50. Alava, T., Mathieu, F., Mazenq, L., Soyer, C., Remiens, D., and Nicu, L. (2010). Silicon-based micromembranes with piezoelectric actuation and piezoresistive detection for sensing purposes in liquid media. J. Micromech. Microeng. *20*, 075014. https://doi.org/10.1088/0960-1317/20/7/075014.

Cell Reports Physical Science, Volume *3*

Supplemental information

Microelectromechanical devices driven by thermosalient effects

Jad Mahmoud Halabi, Isabelle Séguy, Ludovic Salvagnac, Thierry Leïchlé, Daisuke Saya, Fabrice Mathieu, Benjamin Duployer, Durga Prasad Karothu, Liviu Nicu, and Panče Naumov

Supplemental Information

Note S1. Preparation of organic polycrystalline thin films

Multiple methods were tested in investigating the coupling of molecular-crystal actuation with MEMS devices. The goal was to deposit a thin crystalline film of a responsive molecular crystal on silicon-based cantilevers to promote a more robust actuation and easily configurable geometries. Thermosalient compounds based on previous reports and in-lab experiments were considered for the task, including four main candidates: 1,2,4,5-tetrabromobenzene (TBB),[1] naphthalene-2,3-diyl-*bis*(4-fluorobenzoate) (NAPH),[2] phenylpropylammonium bromide (PPB), and L-form of crystalline pyroglutamic acid (LPGA).[3,4] Drop-casting deposition technique was explored but did not yield any reliable and uniform crystalline thin film formation. Contact microprinting method, successfully implemented for spin-crossover materials,[5,6] was also explored where a PDMS device with microchannels was used as a template for crystallization. However, SEM images of the deposited layers showed an absence of a uniform thin crystalline film, and powder X-ray diffraction results also confirmed the lack of substantial crystallinity.

Finally, thin-film deposition through evaporation was considered, based on previous experiments. Even if most evaporated organic molecules display amorphous structures, some of those materials form polycrystalline films. For well-known subliming organic semiconductors like tetracene or pentacene polycrystalline phases have been shown to depend on several factors such as deposition rates, layer thickness, and substrate treatment.[7] However, in some cases, after thermal evaporation, the obtained thin films need to be crystallized by solvent vapor annealing (SVA) post-deposition treatment. Specifically, the molecular spin crossover (SCO) compound $[Fe(II)(HB(tz)_3)_2]$, which displays as-deposited amorphous thin films can be reorganized by SVA using water, ethanol, diethyl ether, dichloromethane, or acetone, while it maintains its spin-transition behavior.[8,9]

SUPPLEMENTAL FIGURES

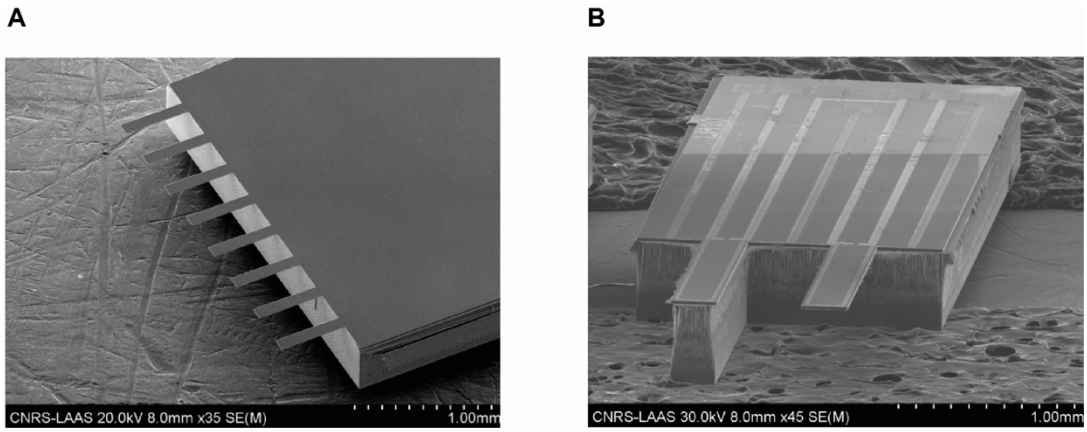

Figure S1. Passive and active microcantilevers. SEM images of an array of (A) passive bare-silicon microcantilevers and (B) active microcantilevers with integrated actuation and detection capabilities.

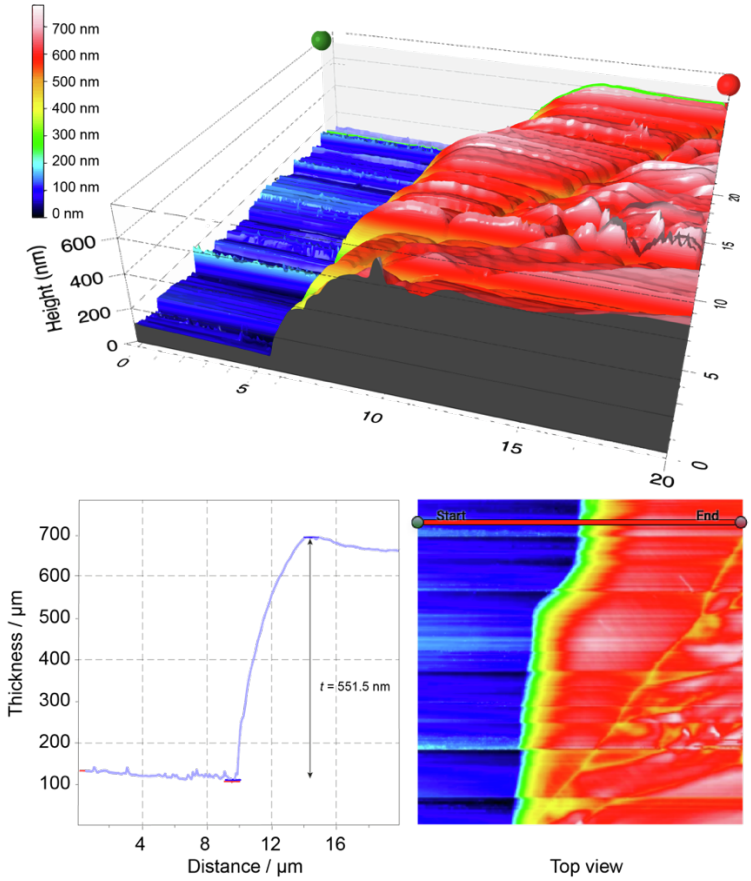

Figure S2. Imaging of LPGA deposited thin-film. AFM imaging of the deposited LPGA thin film on a silicon wafer and the thickness profile along the film cross-section.

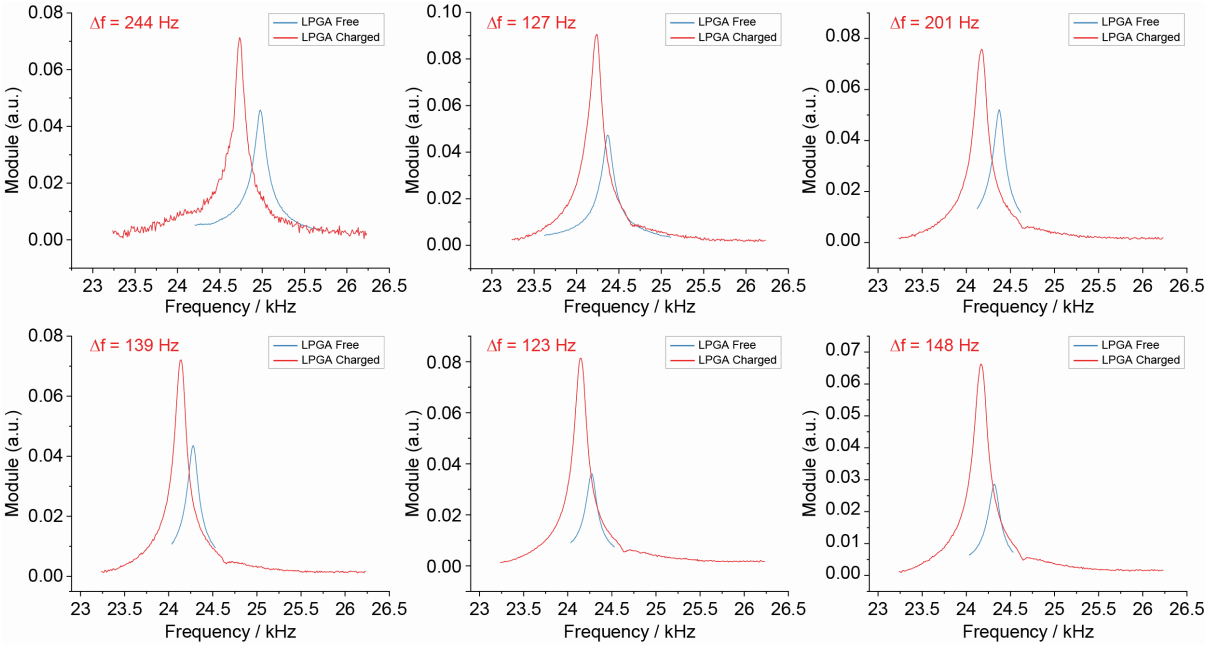

Figure S3. Dynamic frequency measurements for Young's modulus extraction. The shift in resonance frequency between six identical passive microcantilever devices before and after the deposition of LPGA thin film by thermal evaporation.

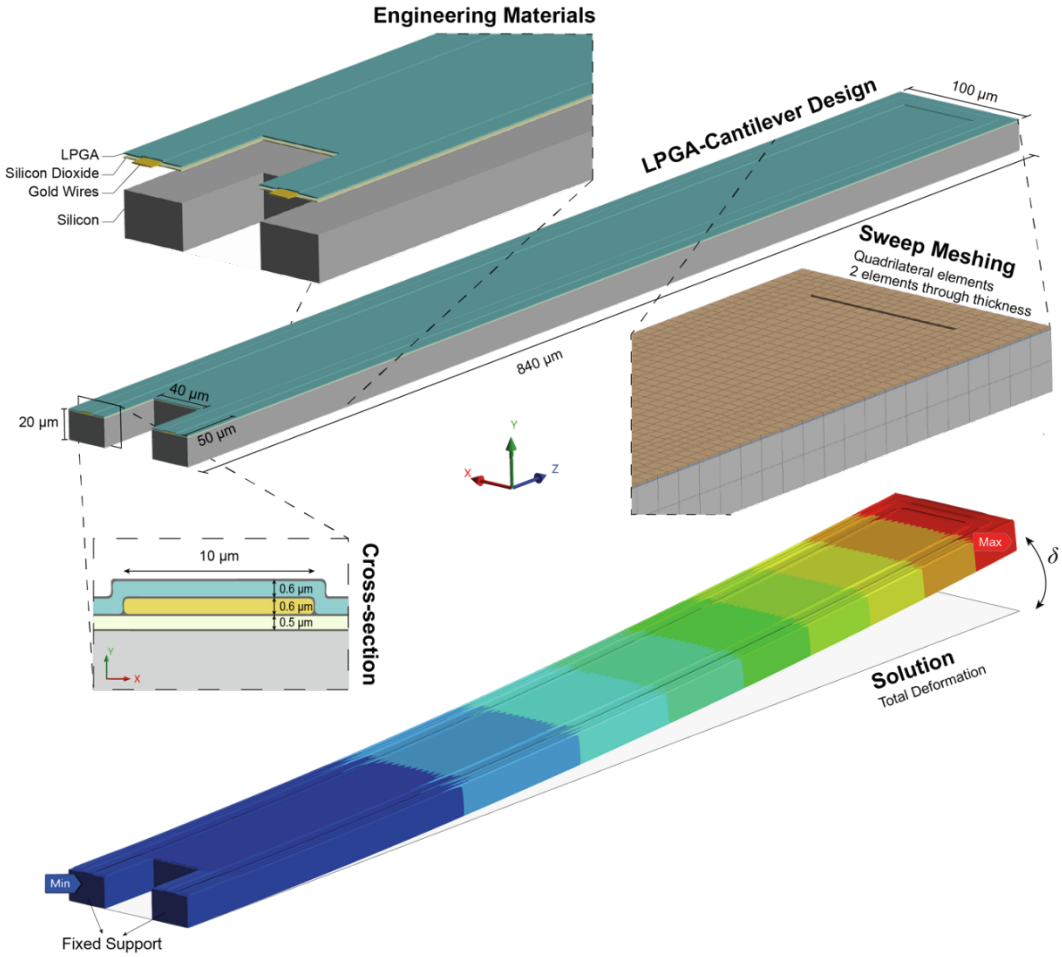

Figure S4. ANSYS Finite Element Analysis modeling. Static structural simulation of the LPGA-charged cantilever bending, quadrilateral meshing of the structure, introduction of materials properties to mimic the experimental setup, and solution color-coded by total deformation during bending.

SUPPLEMENTAL REFERENCES

1. Zaczek, A.J., Catalano, L., Naumov, P. and Korter, T.M. (2019). Mapping the polymorphic transformation gateway vibration in crystalline 1, 2, 4, 5-tetrabromobenzene. *Chem. Sci. 10*, 1332-1341. https://doi.org/10.1039/C8SC03897J.
2. Tamboli, M.I., Karothu, D.P., Shashidhar, M.S., Gonnade, R.G. and Naumov, P. (2018). Effect of crystal packing on the thermosalient effect of the Pincer-type diester naphthalene-2, 3-diyl-bis (4-fluorobenzoate): a new class II thermosalient solid. *Eur. J. Chem. 24*, 4133-4139. https://doi.org/10.1002/chem.201705586.
3. Panda, M.K., Runčevski, T., Husain, A., Dinnebier, R.E. and Naumov, P. (2015). Perpetually self-propelling chiral single crystals. *J. Am. Chem. Soc. 137*, 1895-1902. https://doi.org/10.1021/ja5111927.
4. Karothu, D.P., Mahmoud Halabi, J., Li, L., Colin-Molina, A., Rodríguez-Molina, B. and Naumov, P. (2020). Global performance indices for dynamic crystals as organic thermal actuators. *Adv. Mater. 32*, 1906216. https://doi.org/10.1002/adma.201906216.
5. Quintero, C.M., Il'ya, A., Salmon, L., Molnár, G., Bergaud, C. and Bousseksou, A. (2012). Soft lithographic patterning of spin crossover complexes. Part 1: Fluorescent detection of the spin transition in single nano-objects. *J. Mater. Chem. 22*, 3745-3751. https://doi.org/10.1039/C2JM15662H.
6. Thibault, C., Molnár, G., Salmon, L., Bousseksou, A. and Vieu, C. (2010). Soft lithographic patterning of spin crossover nanoparticles. *Langmuir*, *26*, 1557-1560. https://doi.org/10.1021/la904162m.
7. Nahm, R.K. and Engstrom, J.R. (2017). Who's on first? Tracking in real time the growth of multiple crystalline phases of an organic semiconductor: Tetracene on SiO2. *J. Chem. Phys. 146*, 052815. https://doi.org/10.1063/1.4971288.
8. Bas, A.C., Shalabaeva, V., Thompson, X., Vendier, L., Salmon, L., Thibault, C., Molnár, G., Routaboul, L. and Bousseksou, A. (2019). Effects of solvent vapor annealing on the crystallinity and spin crossover properties of thin films of [Fe (HB (tz) 3) 2]. *C. R. Chim. 22*, 525-533. https://doi.org/10.1016/j.crci.2019.03.002.
9. Manrique-Juarez, M.D., Rat, S., Mathieu, F., Saya, D., Séguy, I., Leïchlé, T., Nicu, L., Salmon, L., Molnár, G. and Bousseksou, A. (2016). Microelectromechanical systems integrating molecular spin crossover actuators. *Appl. Phys. Lett. 109*, 061903. https://doi.org/10.1063/1.4960766.